# Experimental Investigation of Lubrication Regimes of a Water-Lubricated Bearing in the Propulsion Train of a Marine Vessel

**Dov Avishai**
Faculty of Mechanical Engineering,
Technion—Israel Institute of Technology,
Haifa, Israel
e-mail: avishai1@alumni.technion.ac.il

**Groper Morel**
Hatter Department of Marine Technologies,
Leon H. Charney School of Marine Sciences,
University of Haifa,
Haifa, Israel
e-mail: mgroper@univ.haifa.ac.il

*Sliding bearings, operating in a full hydrodynamic lubrication regime, exhibit a low friction coefficient and extended life. In recent years, with the increase in environmental awareness and pollution prevention, attention is being directed to oil spills, which pollute the environment. This is extremely prominent in ships and submarines whose propeller shafts are typically supported by oil-lubricated sliding bearings. To reduce pollution risk and also to obtain a simpler and low-cost maintenance system, the propeller shafts of numerous modern marine vessels are supported by water-lubricated bearings. An experimental investigation into the lubrication regime of a water-lubricated bearing in the propulsion train of a naval vessel is presented. A test rig was designed and built to allow testing of a scaled water-lubricated composite bearing supporting a naval vessel propeller shaft. Experimental results quantifying the effect of the rotational speed on the operating eccentricity, the friction coefficient, and the bearing's lubrication regimes are presented. The experimentally obtained results are compared with an elastohydrodynamic lubrication (EHL) model solved by employing COMSOL MULTIPHYSICS modeling software, and the differences are addressed. Finally, conclusions that may assist in better understanding the operation profile of the bearing and thus improving the vessel's operability are presented.*
[DOI: 10.1115/1.4048382]

*Keywords: elastohydrodynamic lubrication, fluid film lubrication, hydrodynamic lubrication, journal bearings*

## 1 Introduction

**1.1 Theoretical Background.** In recent years [1], with the increase in environmental awareness and pollution prevention, much more attention is being directed to oil spills polluting the marine environment. This heightened the interest is particularly evident regarding marine vessels whose propellers shafts are typically supported by oil-lubricated bearings. To separate the lubricating oil in the vessels' stern tubes from the surrounding seawater, a sealing system based on mechanical or lip seals is typically employed. A failure in this system may result in a situation where oil will leak from the stern tube into the sea, causing a pollution extremely difficult to eliminate.

To avoid this and also to obtain a simpler and almost maintenance-free bearing lubrication system, the propeller shafts of many modern marine vessels such as ships [1,2] and submarines [3,4] are now being supported by water-lubricated fiber resin composite, polymer or rubber made bearings.

This technology requires the use of carefully designed bearings. Several issues that must be considered when designing are as follows: (1) the lower viscosity of seawater in comparison with oils limits the bearings' load carrying capacity in the preferred full hydrodynamic regime, (2) the necessity for efficient flushing of the bearing for cooling and removal of impurities present in seawater requires dedicated longitudinal grooves or other particular geometry, and (3) the possible operation of the bearing in complete or partial contact for extended periods of time and the high corrosiveness of seawater makes the selection of the bearings' materials more challenging than in usual oil-lubricated applications. Ignoring part of these considerations in the design may lead to accelerated bearings' wear and eventually to application failure [2].

Following Striebeck's approach [5], it is common to separate the operation of such bearings into three distinct regimes, in which the bearing may operate at a given time and under certain conditions. (1) In the full hydrodynamic lubrication (HL) regime, the load is totally supported by the pressure field in the thin fluid film entirely separating the rotating journal from the stationary bearing. For complete separation between the journal and the bearing, it is generally accepted [1] that the minimum film thickness $h_0$ should be thicker than approximately $3 \cdot R_q$ (where $R_q$ is the composite rms surface roughness, $R_q = \sqrt{R_j^2 + R_b^2}$). (2) In the mixed lubrication (ML) regime, the load is partially supported by the pressure field in the fluid film and partially by direct contact between asperities. The acceptable range for minimum film thickness in this regime is $1.0 \cdot R_q < h_0 < 3 \cdot R_q$ [6]. (3) Finally, in the boundary lubrication (BL) regime, the load is entirely supported by contact between asperities. Here, the minimum lubricant film thickness is in the order of $h_0 \leq 1.0 \cdot R_q$.

In the latter regime, direct contact between asperities causes a significant increase in the friction coefficient, the power loss, and the bearing's and journal's wear. We also hypothesize that bearings operating in the full hydrodynamic regime are quieter than those operating in the mixed or boundary lubrication regimes. Although not directly proved, a similar hypothesis was also suggested in Refs. [3,4]. This may be of importance in naval vessels such as in underwater vehicles where the noise emitted into the medium should be minimized.

Solution of the Reynolds equation subject to typical assumptions [5] provides the pressure field in the lubrication film. Accordingly,

Contributed by the Tribology Division of ASME for publication in the JOURNAL OF TRIBOLOGY. Manuscript received May 8, 2020; final manuscript received August 7, 2020; published online September 28, 2020. Assoc. Editor: Ramin Rahmani.

  

knowledge of the pressure field allows evaluation of the bearing performance parameters (load carrying capacity, friction coefficient, etc.). Nevertheless, in a polymer journal bearing with a low Young's modulus as typically employed in marine water-lubricated bearings [2,7], the bearing's elastic deformation affects the hydrodynamic pressure and vice-versa. Therefore, an elastohydrodynamic lubrication (EHL) solution model should be applied.

An EHL theoretical model of a polymer partial journal bearing operating in the full hydrodynamic lubrication regime involves the coupling of two models: a fluid dynamic-based model for the lubricant film and a solid mechanics model for the bearing material. The first model is of a creeping flow of a thin lubricant film in a narrow converging/diverging gap which is responsible for the pressure field buildup in the bearing. This model is described by the Reynolds equation. The second model examines the influence of the lubricant pressure field on the bearing's material deformations, which are described by Hooke's law. In case of a polymer bearing, deformations may locally alter its shape and influence the pressure distribution.

Oh and Huebner [8] were among the first to propose a solution to the EHL problem and their work formed the basis for additional researches in the last decade. Litwin [7] focused his work on water-lubricated bearings installed in marine vessels and proposed an algorithm to solve the coupled physics, fluid–structure, in these bearings. De Kraker et al. [9] presented a mixed EHL model for water-lubricated journal bearings and computed Stribeck's curves. They employed a finite element method to solve the coupled fluid–structure equations. This model was later employed by Hirani and Verma [2] to compute the pressure distribution in water-lubricated bearings installed in the shaft train of some Indian Coast Guard vessels. Recently, in a comprehensive numerical study, Xie et al. [10] used computational fluid dynamics to investigate the effects of fluid–structure interaction on water-lubricated bearing performances employed in the primary circuit loop system of a nuclear power plant. The influence of the rotating speed, eccentricity ratio, bushing thickness, and lubrication models were investigated and presented.

Analytical solutions for partial arc journal bearings, such as the one considered in the present study, were presented by Pinkus and Sternlicht [11] and Yu and Szevi [12] while assuming a long bearing ($L/D > 2$) approximation. Malik et al. [13] presented a numerical, finite differences solution for the pressure field in a finite partial bearing using pseudoplastic lubricants.

**1.2 Experimental Studies.** The earliest recorded experiments on lubricated journal bearings are from the 19th century. The first to investigate these bearings was Tower [14] in 1883. His celebrated experiments were the first to present the hydrodynamic pressure field in a thin lubricant film of a journal bearing. Basing themselves on Tower's findings, numerous experimental studies on journal bearings such as McKee et al.'s [15–17] were published in the middle of the 20th century. These works focused on oil-lubricated metal bearings. Toward the end of the 20th century, with the progress in composite polymer materials, researchers began to experimentally investigate bearings made of different materials and employing water as the lubricating fluid. Sprengel and Hargreaves [18] were among the first to study nonmetallic journal bearings using water as the lubricating fluid.

In recent years, experimental works investigating the influence of geometry on the load carrying capacity [19]; the effect of the clearance, bearing material, and lubricating grooves [20]; and the impact of the liquid properties [21] on the bearing's performance were published. Some of the experimental works were performed on test rigs allowing testing of a complete radial bearing, while other studies focused on testing a specimen. Litwin [22] performed experimental investigations on the operational performance for oil- and water-lubricated bearings. Experiments on two full-scale partial marine water-lubricated bearings show that at low speed a full lubricating film usually does not form and that the bearings operate in the ML regime. Hongling et al. [3] used the water-lubricated bearing test rig SBB-100 to study the influence of the rotating speed, contact pressure, material hardness, and thickness on the induced vibration on a specimen extracted from a stern tube bearing.

Recently, Xie and Liu [4] presented an experimental work on the influence of surface roughness and operational conditions on the transition between lubrication regimes in a water-lubricated bearing employed in the propulsion system of an underwater marine vehicle. They designed and developed a test rig with a complete radial bearing in an overhung configuration submerged in a water tank. In their test rig, the bearing's frictional torque was computed by measuring the tangential force on a force arm.

In experimental works employing a complete radial journal bearing, the test rig typically [3,22,23] consists of a shaft supported by two rolling element or hydrostatic bearings rotated by an AC motor with speed and torque monitoring systems. In most configurations, a loading system equipped with a load cell sensor was used to load the stationary bearing [22,23], while in another study [19], the loading system loaded the rotating shaft.

A lubrication system employing a motor-driven pump, piping, fittings, a monitoring system and often a heat exchanger were used to pump the lubricating fluid from a dedicated container into the bearing. In most cases, the bearing's eccentricity was measured by eddy current sensors. Pressure sensors used to measure the pressure in the thin film were mounted in dedicated ports drilled in the stationary bearing [21] or in the rotating shaft and employing a wireless transmission system [19].

The present investigation used all these systems and sensors in designing the test rig, aiming to have the most beneficial configuration.

Here, we study a water-lubricated journal bearing supporting the main shaft of a naval vessel. Noise emitted from this bearing accompanied by accelerated wear has heightened the necessity for determining its rotational speed relative to the respective operational lubrication regime. The bearing under investigation is a partial bearing of a 100 deg sector, with a diameter of 400 mm and a length of 1200 mm. The nominal radial clearance between a new bearing and a new journal is 0.6 mm. Through its entire rotational speed range, 40–200 rpm, the bearing supports an approximately constant load of 70 kN. The bearing is made of a resin composite polymer material, RAILKO NF22, with properties presented in Table 1. Based on vessel's crew reported findings, emitted noise, and accelerated wear, it was postulated that the bearing, for some of the rotational speed range, may not operate in the desired full hydrodynamic regime. To study the operation of the aforementioned bearing and to test this hypothesis, a numerical EHL model for a partial bearing was developed and a test rig for experimental testing of the bearing operation was designed and constructed. Based on the numerical and experimental results, conclusions about the bearing's operational regime are presented.

**Table 1 RAILKO NF22 material properties**

| Property | Units | Value |
|---|---|---|
| Density | g/cm$^3$ | 1.64 |
| Ultimate compressive strength | MPa | |
| Radial | | 176.5 |
| Axial | | 98 |
| Maximum working compressive strength | MPa | |
| Radial | | 44 |
| Axial | | 24.5 |
| Ultimate tensile strength | MPa | 30.4 |
| Compressive modulus | MPa | 4020 |
| Shear strength | MPa | 41 |
| Maximum working temperature | °C | 100 |
| Coefficient of friction (dry) | – | 0.25–0.4 |
| Hardness (HB) | Brinell | 29 |
| Swell in water at 20 deg | % | <1 |

## 2 Theoretical Analysis

**2.1 Terminology.** Figure 1 presents the terminology for a partial hydrodynamic bearing operating in the full hydrodynamic regime. $R$ represents the bearing {1} radius, and $r$ represents the journal {3} radius. The journal is loaded by a load $W$ and rotates with a rotational speed $N$. The density and the viscosity of the lubricant {4} is $\rho$ and $\mu$, respectively. The bearing's external housing is denoted by {2}.

In a partial arc journal bearing, such as the one considered in the present study, only an angular sector $\Delta\theta$ of a whole cylindrical bearing exists, starting at angle $\theta_{start}$ and ending at $\theta_{end}$. The circumferential coordinate $\theta$ is measured from the line of centers $(O_b - O_j)$. The attitude angle $\phi$ is the angle between the load line and the line of centers and $e$ is the eccentricity between the journal's and bearing's centers'.

The film thickness $h(\theta)$ is described by the term $h(\theta) = C(1 + \varepsilon \cos\theta)$, where $C$ is the radial clearance and $\varepsilon$ is the dimensionless eccentricity $\varepsilon = e/C$. The minimum film thickness $h_0 = C(1 - \varepsilon)$ occurs at $\theta = \pi$.

**2.2 Model.** In the present work, the numerical solution for the EHL problem of a finite, partial composite bearing is presented.

Figure 2 presents the employed model, where a journal rotates against a static composite partial bearing with a thin lubricant film between the surfaces. Due to the hydrodynamic pressure in the film, local elastic deformation occurs on the bearing's surface, which influences the hydrodynamic pressure in the fluid film. For an accurate estimation of the bearing's performance, the elastic deformation needs to be calculated and included in the Reynolds equation (Eq. (1)):

$$\frac{\partial}{\partial x_1}\left[h^{*3}\frac{\partial p}{\partial x_1}\right] + \frac{\partial}{\partial x_3}\left[h^{*3}\frac{\partial p}{\partial x_3}\right] = 6\mu U\frac{\partial h^*}{\partial x_1} \tag{1}$$

where $h^*$ stands for the local radial clearance that includes the local deformation $u$ of the bearing (Eq. (2)).

$$h^*(x_1, x_3) = h(x_1) + u(x_1, x_3) \tag{2}$$

Four boundary conditions (BCs) are required for the solution of the Reynolds equation (Eq. (1)) with the local radial clearance given in Eq. (2). As the Reynolds equation for a partial, finite journal bearing with a deformed shape cannot be solved analytically, a numerical solution will be employed. Since no actual misalignment data between shaft and bearing were available, axial symmetry of the bearing is assumed and only half the bearing is solved. Consequently, the BCs are given as follows:

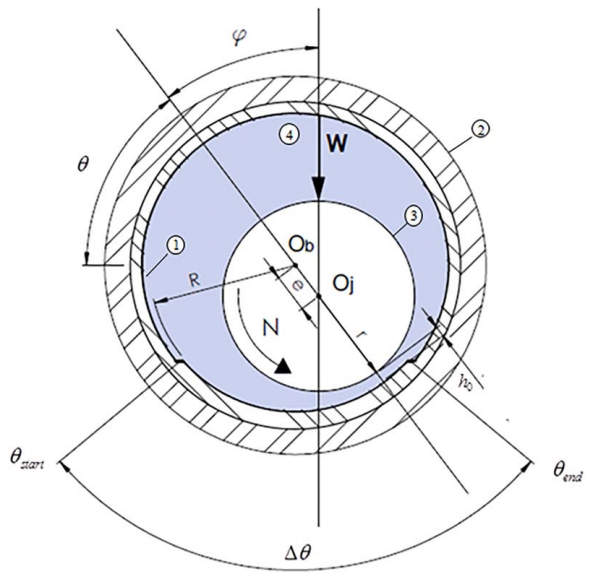


**Fig. 1 Terminology for a partial hydrodynamic bearing operating in the full hydrodynamic regime**

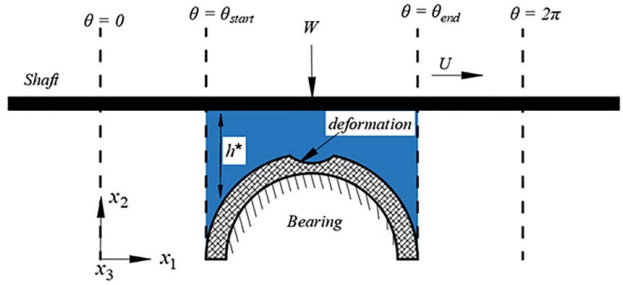


**Fig. 2 Unwrapped film shape in a partial bearing including deformations**

At $\theta = \theta_{start}$ and $\theta = \theta_{end}$, the pressure equals the ambient pressure, $p_s$:

$$p(x_1 = R\theta_{start}, x_3) = p_s \tag{3}$$

$$p(x_1 = R\theta_{end}, x_3) = p_s \tag{4}$$

As the bearing is submerged, its edges are also subjected to the ambient pressure. Thus:

$$p(x_1,\ x_3 = 0) = p_s \tag{5}$$

The symmetry condition at the bearing's longitudinal center is given by

$$\frac{\partial p}{\partial x_3}(x_1,\ x_3 = L/2) = 0 \tag{6}$$

As the bearing includes a diverging zone, the possibility of cavitation should be incorporated. For the cavitation region, the Swift and Stieber [5] condition is employed (Eq. (7)):

$$\begin{aligned} p(x_1 = R\theta_{cav}, x_3) &= p_{cav} \\ \frac{\partial p}{\partial x_1}(x_1 = R\theta_{cav}, x_3) &= 0 \end{aligned} \tag{7}$$

The elastic deformation of the bearing's surface caused by the pressure in the lubricant film is calculated by employing Hooke's law, strain–displacement, and the force equilibrium equations.

A possible scheme to solve the EHL problem is presented in Fig. 3. The scheme starts by employing an initial guess for the attitude angle and the dimensionless eccentricity to calculate the pressure field in the lubricant film. The obtained pressure is used to calculate the elastic deformations in the bearing. The film thickness is updated accordingly, and the computation continues in an iterative process until convergence on the film thickness, the load carrying capacity, and the attitude angle are achieved. In this study, the EHL model is solved using COMSOL MULTIPHASIC® modeling software, which is based on the finite element method.

For solving the coupled EHL problem, for the fluid film and the solid bearing, the bearing is developed into a smooth plate with thickness $T$, length $L/2$, and width $(\theta_{end} - \theta_{start}) \cdot 2\pi R$, as presented in Fig. 4. The Reynolds equation (Eq. (1)), fluid boundary conditions (Eqs. (3)–(6)), and the cavitation condition (Eq. (7)) were defined on the surface interfacing with the fluid using COMSOL MULTIPHASIC's® equation-based modeling package. The displacement field in the solid bearing was calculated using COMSOL's Structural Mechanics module by defining the boundary conditions on the outer surface, fluid interfacing surface, and symmetry surface. Tetrahedral elements were applied in the discretization of the bearing's volume, which resulted in triangular elements on the bearing's face interfacing with the fluid film. Repetitive computations ware

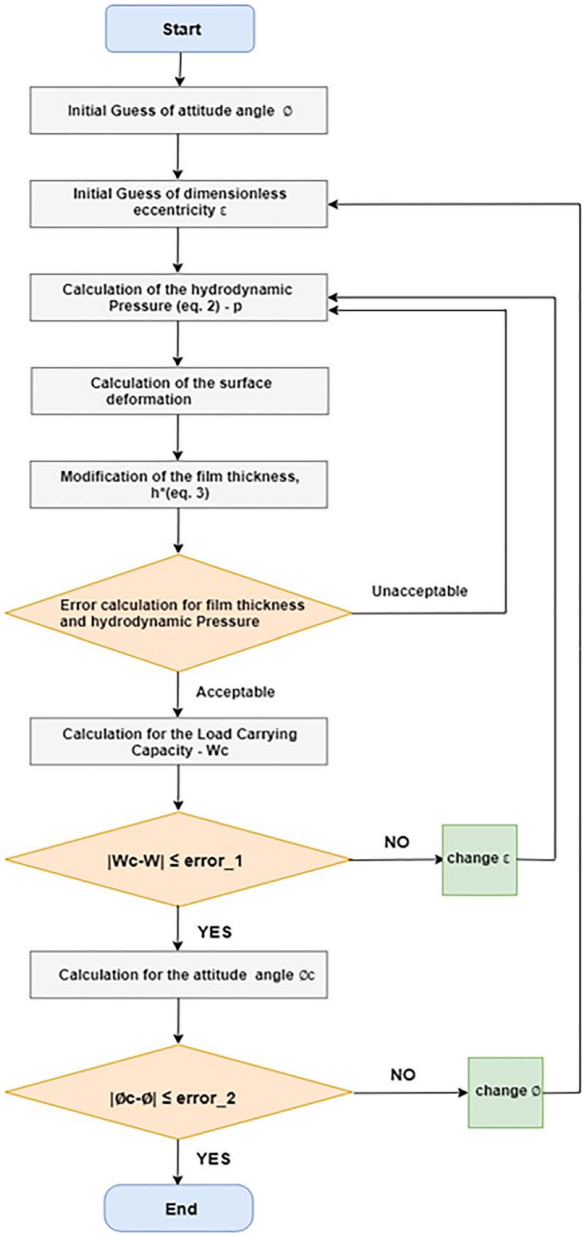


**Fig. 3 Scheme for estimating the performance of a partial elastic bearing**

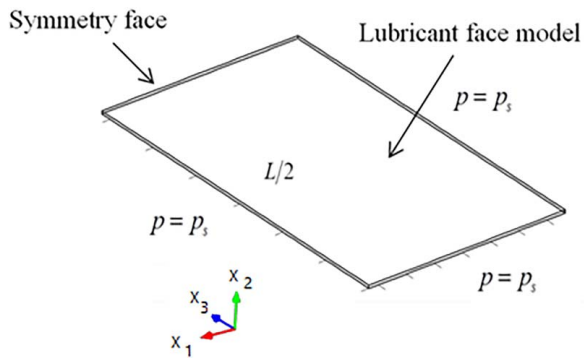


**Fig. 4 Bearing developed into a flat plate: lubricant–film bearing interface**

**Table 2 Convergence error versus grid quality**

| Grid quality | Number of elements | Convergence error (%) |
|---|---|---|
| Coarser | 2823 | – |
| Coarse | 5582 | 9 |
| Normal | 12,790 | 3 |
| Fine | 23,033 | 2 |
| Finer | 30,668 | 0.3 |
| Extra fine | 47,930 | 0.3 |

performed for six mesh qualities (coarser, coarse, normal, fine, finer, and extra fine). The last two meshes (fine and extra fine) provided identical results, and thus, we determined the mesh quality for further use. Details of convergences versus grid quality are provided in Table 2.

The fluid branch, using the COMSOL MULTIPHASIC's® equation-based modeling package, is iteratively updated with the modified local radial clearance, $h^*$ (Eq. (2)), which includes the elastic deformation.

The pressure and the displacement fields are calculated until convergence is achieved. In this study, convergence was typically achieved using the Newton–Raphson method over 60 iterations with a monotonic decrease in error after each iteration.

Given that the bearing should support a given constant load, an iterative process for load and attitude angle calculation until convergence was further applied. Consequently, a MATLAB code interfacing with COMSOL API was developed.

**2.3 Results.** The EHL model results as obtained using the COMSOL MULTIPHASIC® software are presented in Table 3 and in Figs. 5–8.

The friction coefficient numerically obtained using the EHL model is presented in Table 3. As expected, when the shaft rotational speed is increased, the friction coefficient also increases. This increase in the friction coefficient is explained by the increase in the shear stress in the lubricant, which characterizes the full hydrodynamic lubrication regime.

At a low journal rotational speed, the pressure field extends to a narrow angular section, but the maximum pressure (pressure peak) is high (Fig. 5(*a*)). Conversely, when the rotational speed is increased, the pressure field extends to a larger angular section, but the maximum pressure is lower (Fig. 5(*b*)). This pressure field shape is explained by the fact that the load applied on the journal is constant regardless of the rotational speed. Thus, when the rotational speed is low, the eccentricity is high and the pressure field is narrow with a high peak. Conversely, the higher the rotational speed is, the lower the eccentricity is, resulting in the pressure field widening and the maximum pressure dropping.

The shape of the deformation field resembles the pressure field, as presented in Figs. 7 and 8. At low rotational speed, higher deformations occur in a narrower angular sector (Fig. 8(*a*)), while when the rotational speed is increased, the deformation sector grows larger with smaller deformations (Fig. 8(*b*)).

The polymer bearing evaluated in this work exhibits a maximum radial displacement of circa 0.5 $\mu$m, one order of magnitude smaller than the film thickness. Consequently, in this study, a rigid bearing

**Table 3 EHL solution—friction coefficient, vessel's bearing**

| Rotational speed, $N$ (rpm) | Friction coefficient, $f$ |
|---|---|
| 40 | $4 \times 10^{-4}$ |
| 60 | $5 \times 10^{-4}$ |
| 80 | $6 \times 10^{-4}$ |
| 120 | $7 \times 10^{-4}$ |

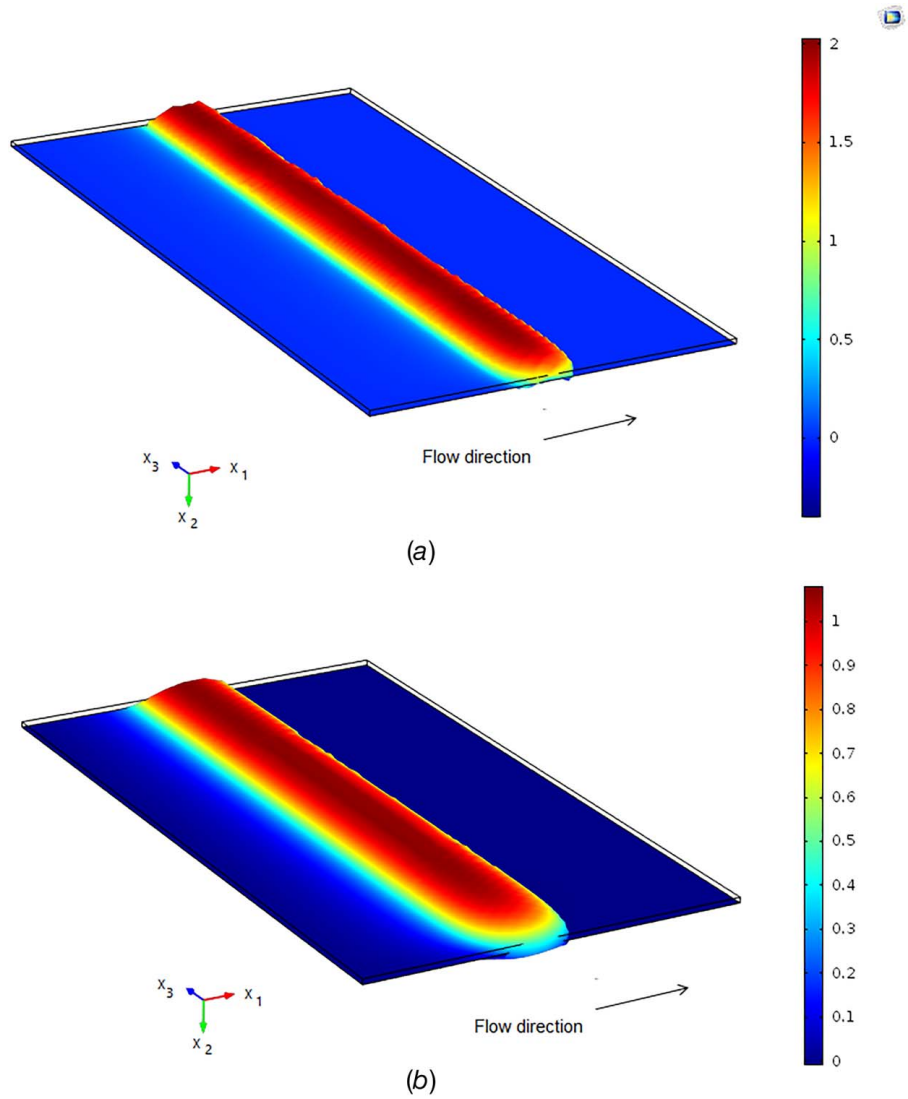


**Fig. 5 Pressure field in the unwrapped bearing: (*a*) $N = 40$ rpm and (*b*) $N = 200$ rpm**

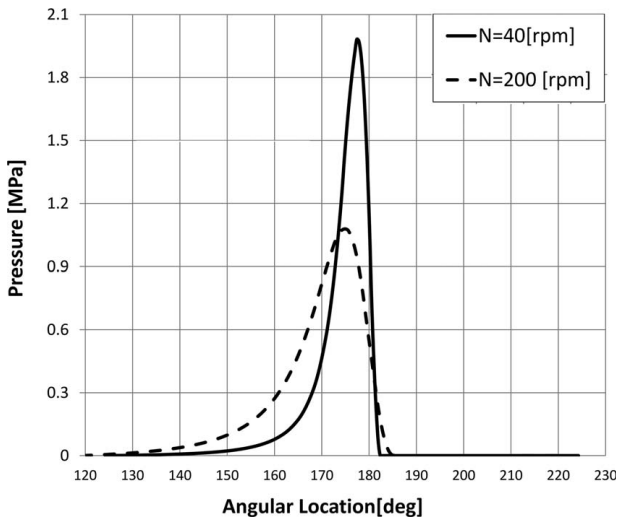


**Fig. 6 Hydrodynamic pressure distribution as a function of the rotational speed in the film at the bearing's middle cross section**

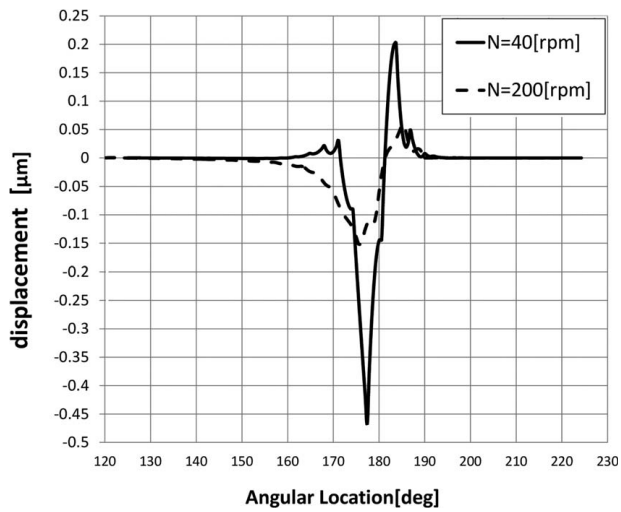


**Fig. 7 Radial displacement as a function of the rotational speed in the polymer at the bearing's middle cross section**

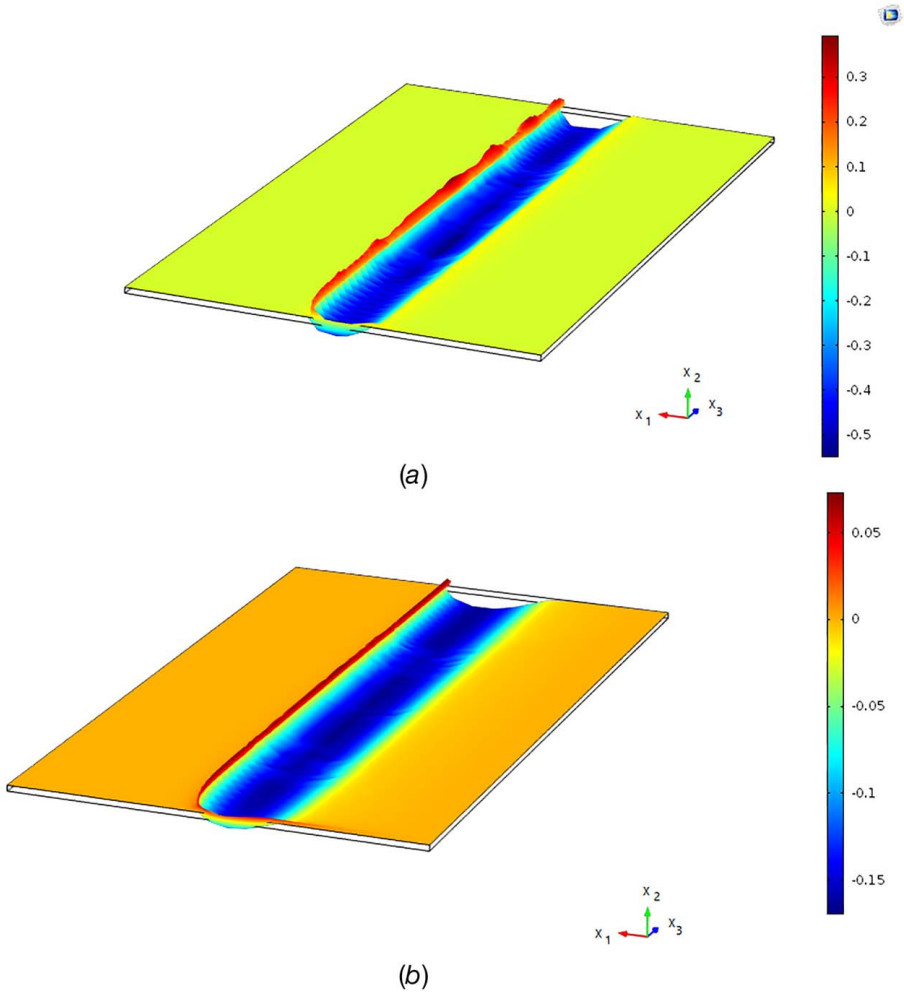


**Fig. 8 Displacement field in the unwrapped bearing: (*a*) $N = 40$ rpm and (*b*) $N = 200$ rpm**

assumption could be made, leading to a relatively small error in the evaluation of the bearing's performance.

## 3 Experimental Investigation

**3.1 Investigated Bearing.** This study focuses on a bearing used in supporting a vessel's main propeller shaft. The diameter of the propeller shaft is 400 mm, and its rotational speed is in the range of 40–200 rpm. Similar to the previous works [19,23], due to design and physical constraints, we believe that the test rig shaft diameter should not exceed 100 mm. Consequently, similarity between the vessel's bearing and the investigated bearing in our test rig was maintained by using the Buckingham π theorem and the relevant dimensionless parameters.

The load carrying capacity of a rigid partial journal bearing is a function of the lubricant viscosity, the bearing's radius and length, the journal rotational speed, the radial clearance, the eccentricity, and the bearing's angular sector:

$$W = f(\mu, R, L, N, C, e, \theta_{start}, \theta_{end}) \tag{8}$$

The dimensionless parameters we preserved were the Sommerfeld number (Eq. (9)), the length-to-diameter ratio $\lambda$, the dimensionless eccentricity ($\varepsilon = e/C$), the radial clearance-to-radius ratio ($C/R$), and the angular sector of the bearing $\Delta\theta$.

$$S = (\mu N/p_{av}) \cdot (R/C)^2 \tag{9}$$

In addition, the average pressure $p_{av} = W/(L \cdot 2R)$ and the tangential velocity $U$ in the bearing employed in the test rig were kept identical to those of the vessel's bearing. Finally, as we employed potable water as the lubricant, a viscosity correction between seawater and freshwater was introduced. Based on these similarity considerations, the dimensions and operational parameters for the experimental bearing were obtained and presented in Table 4.

**3.2 Test Rig.** The test rig designed and developed for the experimental investigation of the water-lubricated bearing is presented in Fig. 9. A 5.5 kW AC induction motor {1} propels the test rig's main shaft {2}. The shaft is supported by two double-row spherical roller bearings {3} and is connected to the motor through two elastic couplings {4}. A torque meter {5}, installed between the two couplings, measures the rotational torque required to rotate the shaft and, following a calibration procedure later described, permits computation of the hydrodynamic frictional torque and consequently the coefficient of friction.

**Table 4 Experimental bearing dimensions and operational data**

| Dimension/operational parameter | Units | Value |
|---|---|---|
| Diameter | mm | 75 |
| Length | mm | 230 |
| Radial clearance | mm | 0.26 |
| Load | kN | 2.5 |
| Shaft rotational speed | rpm | 80–1000 |

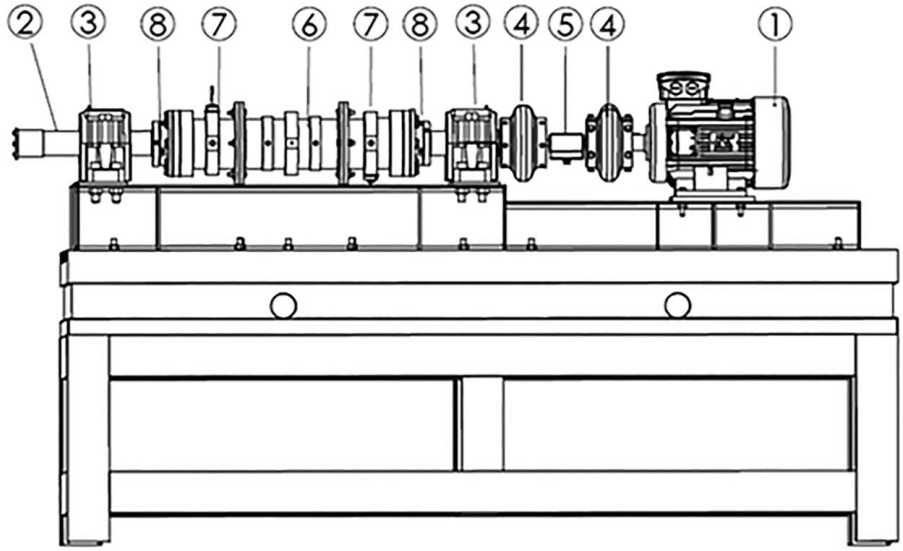


**Fig. 9 Test rig—general arrangement**

The experimental journal bearing was fitted in a dedicated cylindrical machined housing {6} and located centrally between the support bearings. To imitate the submerged operational configuration of the bearing, water volumes {7} were machined and installed on both sides of the journal bearing housing. Sealing between the rotating shaft and the stationary water volumes is achieved using low friction mechanical seals {8}. A submerged water pump drains water from a 200-l container and discharges through the supply hose connected to one of the water volumes. Exiting the first water volume, the water circulates through the bearing to the opposite water volume, from where it is returned to the water container through the return hose. A globe valve on the return hose is used to set the water flow and pressure. Resistance temperature detectors were installed in both water volumes to measure the supply and return water temperature.

The bearing's loading system is presented in Fig. 10. A slender rod {1} connects the bearing housing to a worm gear hand-operated screw jack {3}. To permit delicate adjustment of the applied load, a spring {2} was installed between the rod and the screw jack to act as a high displacement-to-force ratio transmission system. A load cell {4} mounted just between the spring and the rod measures the applied load. As the long rod is extremely pliable, the bearing assembly basically floats over the shaft and is free to move horizontally. This option is essential since the bearing must be allowed to achieve its natural attitude without additional constraints. We also emphasize that contrary to the configuration of the vessel's propeller shaft where the shaft is loaded and free to move in the bearing, here the shaft is restrained between the rolling element bearings and the load is applied to the bearing, which is also free to displace over the shaft and attain its operational location (eccentricity). This configuration is similar to configurations described in the previous works [7,23].

A partial longitudinal cross section of the shaft {1} with the journal bearing {2} fitted in its housing and connected to one of the two water volumes {3} is presented in Fig. 11. Tightness between the bearing housing and the water volume is achieved by a static O-ring seal. The mechanical seals {4} seal the water basins while allowing the shaft to rotate. One of the two rolling element bearings {5} supporting the shaft {1} is also shown.

Three pressure transducers {6} were threaded into three long channels axially bored in the shaft. Radial ports were bored in three distinctive axial and angular locations along the shaft beneath the journal bearing, each connected to one of the three axial channels. It was believed that this design would permit continuous circumferential monitoring of the pressure in the lubricant film at three distinctive locations along the bearing. Unfortunately, this configuration did not operate satisfactorily, and the obtained pressure readings were not reliable. It is assumed that the erroneous readings were a result of some unexpected compressibility in the measuring system, conceivably as a result of residual trapped air in the channels without a feasible possibility of being eliminated. Two proximity sensors {8}, mounted in a 90-deg configuration, were installed in each of the two water volumes to measure the shaft orbit and calculate the average operational eccentricity. All test rig sensors are listed in Table 5.

As a major parameter goal of the experimental phase was to obtain the journal bearing's friction coefficient by measuring its friction torque, the parasitic friction torque produced by other rotation components in the test rig had to be estimated in a separate calibration phase and further eliminated accordingly. The friction coefficient of the rolling element bearings {5} was obtained by measuring their parasitic torque with the water-lubricated bearing {2}, and the mechanical seals {4} were removed from the test rig

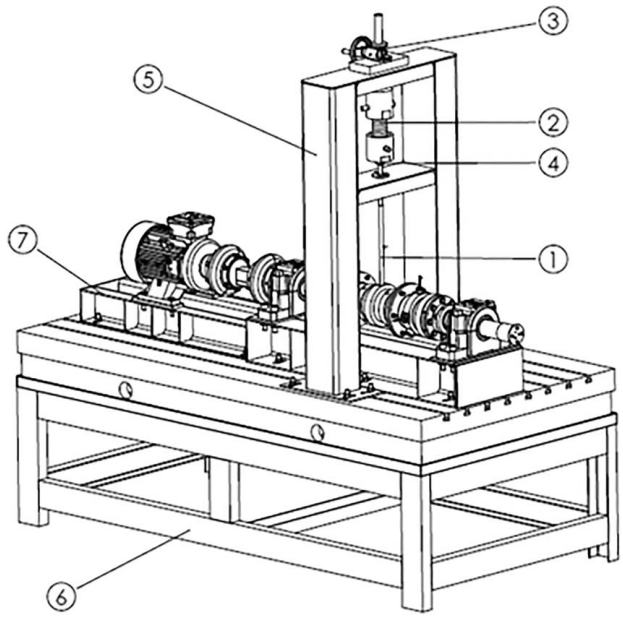


**Fig. 10 Test rig—bearing loading system**

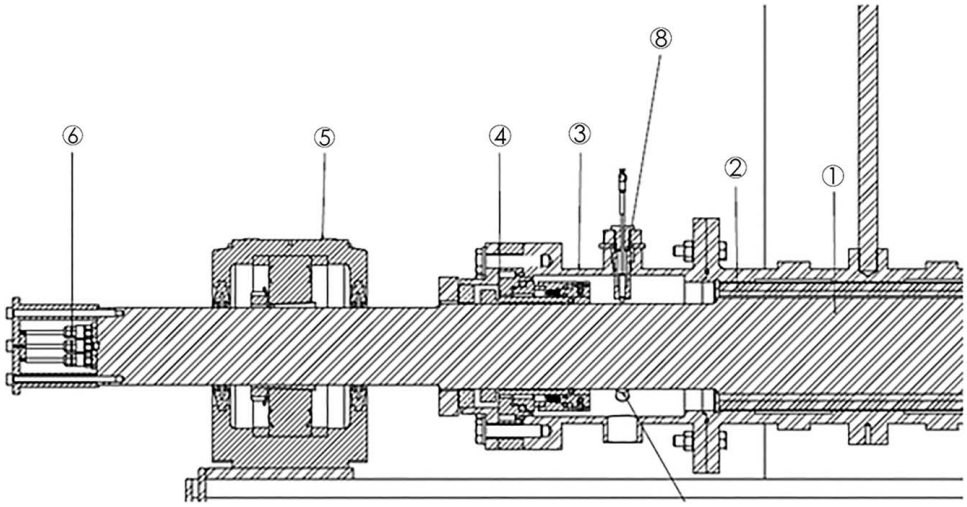


**Fig. 11 Test rig—pressure and proximity sensors location**

and the rolling element bearings loaded by the shaft self-weight only. The main contributor to the parasitic torque is the mechanical seals. Their friction torque was measured in a dedicated experiment performed with the water-lubricated bearing removed from the test rig and their parasitic friction torque measured at the relevant rotational speeds.

**3.3 Results.** The present work sought to investigate the performance of the bearing, in particular to detect if and under which shaft rotational speeds the bearing does not operate in the preferred full HL regime. The presented experimental results are based on the measurements of torque and shaft eccentricity as obtained from the torque and proximity sensors. Raw data obtained from the torque sensor were filtered and postprocessed to remove parasitic torque created by the other components of the test rig (rolling element bearings and mechanical seals) and noise. The raw data obtained from the proximity sensors were postprocessed to compensate for the previously measured DC offset and to remove noise. In all measurements, the bearing was operated under a constant nominal load of 2.5 kN, which matches the load on the vessel's bearing. The shaft rotational speed was maintained in the range of 200–1100 rpm, again matching the rotational speed of the vessel's shaft. All the presented results are average values of numerous experiments performed using an identical configuration.

*3.3.1 Friction Coefficient.* The experimentally obtained results for the frictional torque in the journal bearing $T_f$ allowed the computation of the friction coefficient $f$ by employing the following expression:

$$f = \frac{T_f}{W \cdot R} \tag{10}$$

For lower shaft rotational speeds, the obtained friction coefficients were high, on the order of 0.1, which suggests operation in the BL regime. As the shaft rotational speed was increased, the friction coefficient decreased to values in the order of 0.001. Reduction of the friction coefficient as the shaft's rotational speed increases suggests the development of hydrodynamic effects in the bearing, i.e., transfer to a ML regime. As the shaft rotational speed was further increased, at approximately 700 rpm, the friction coefficient started, very moderately, to increase. This increase in the friction coefficient may be explained by the increase in the shear stress in the lubricant, which characterizes the full HL regime. Figure 12 presents the change in the friction coefficient versus the shaft rotational speed as obtained in the experiments performed and outlines, approximately, the three lubrication regimes under which the investigated bearing operates.

*3.3.2 Minimum Clearance Estimation.* Figure 13 depicts the experimentally obtained minimum clearance between the stationary bearing and the rotating shaft as a function of the shaft rotational speed ($N$). All results are for the nominal load of 2.5 kN. At approximately 300 rpm, the measured minimum clearance was in the order of 0.3 $\mu$m. As the shaft rotational speed was increased, the clearance grew monotonically and reached an approximated value of 7.5 $\mu$m at 1100 rpm. A film thickness coefficient $\Lambda$ may be calculated using the following expression:

$$\Lambda = \frac{h_0}{\sqrt{R_j^2 + R_b^2}} \approx \frac{h_0}{R_b} \tag{11}$$

where $h_0$ is the minimum clearance (film thickness), and $R_j$ and $R_b$ are the steel shaft and polymer bearing average surface roughness, respectively. As the shaft surface was polished to an average roughness value of $R_j = 0.1$ $\mu$m and the bearing surface roughness as reported by the bearing's manufacturer was of the order of $R_b =$ 2.5 $\mu$m, the shaft surface roughness is neglected in the expression for the film thickness coefficient.

For a rigid oil-lubricated metal bearing, it was estimated [1] that the full hydrodynamic regime commences when $\Lambda > 3$ approximately. Nevertheless, previous works that investigated polymer bearings [7] showed that a full hydrodynamic regime may

**Table 5 Test rig sensors**

| Sensor | Company | Model | Measured parameter | Calculate parameter | No. of sensors |
|---|---|---|---|---|---|
| Torque meter | Honeywell | 1700 | Torque and shaft rotational velocity | Friction coefficient | 1 |
| Proximity sensors | Lion precision | U5C & ECL202 | Local distance from the shaft | Eccentricity | 4 |
| Temperature | Electroterm | PT-100 | Water temperature | Water viscosity | 2 |
| Pressure transducers | MEAS | XP1128 | Pressure | Pressure | 3 |
| Load cell | InterFace | WMC-1K | Force | Load | 1 |

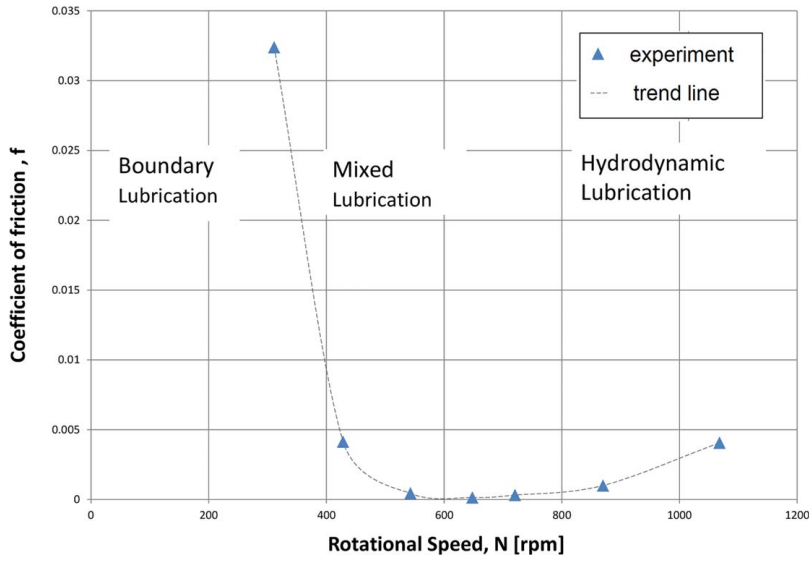


**Fig. 12 Coefficient of friction (*f*) versus rotational speed (*N*) for the experimental bearing**

commence at a lower film coefficient value than in metal bearings and was estimated to be at $\Lambda > 2$. It was postulated that this may be due to surface wear that occurs in the running-in period, causing the bearing's surface to be polished and resulting in an improvement in its surface roughness. Based on the friction coefficient values as detailed earlier, the estimated lubrication regimes are shown in Fig. 13. In addition, for each regime, the average film thickness coefficient was noted. As can be observed, a full hydrodynamic lubrication regime commences at a film thickness coefficient of approximately 2.

## 4 Results Comparison and Discussion

We now compare the friction coefficient numerically obtained for the investigated bearing using the EHL model with the experimental results presented in Fig. 12. This comparison is presented graphically in Fig. 14.

In the low-speed range, i.e., below 500 rpm, the experimentally obtained values for the friction coefficient are significantly higher than the computed ones generated by the EHL model. For example, at 300 rpm, a value of 0.03 was obtained experimentally, while the EHL model predicted a value of 0.002. This significant difference is relatively easy to explain. The EHL model is based on Reynolds' theory, which is valid in the full HL regime only. This model does not account for the applicability of the calculated minimum clearance and assumes that a full hydrodynamic film can be established for every clearance. For the cases where the clearance is narrower than the equivalent surface roughness, however, a full hydrodynamic film cannot develop.

Consequently, the bearing will operate in the mixed or even boundary lubrication regime with a higher friction coefficient. At higher rotational speeds, above approximately 500 rpm, a good

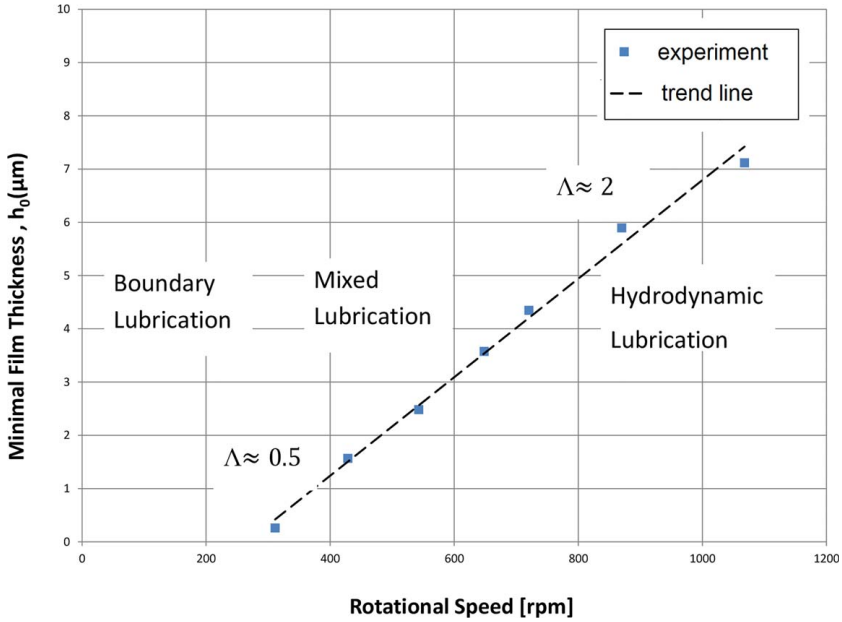


**Fig. 13 Minimal film thickness ($h_0$) versus shaft rotational speed (*N*) for the experimental bearing**

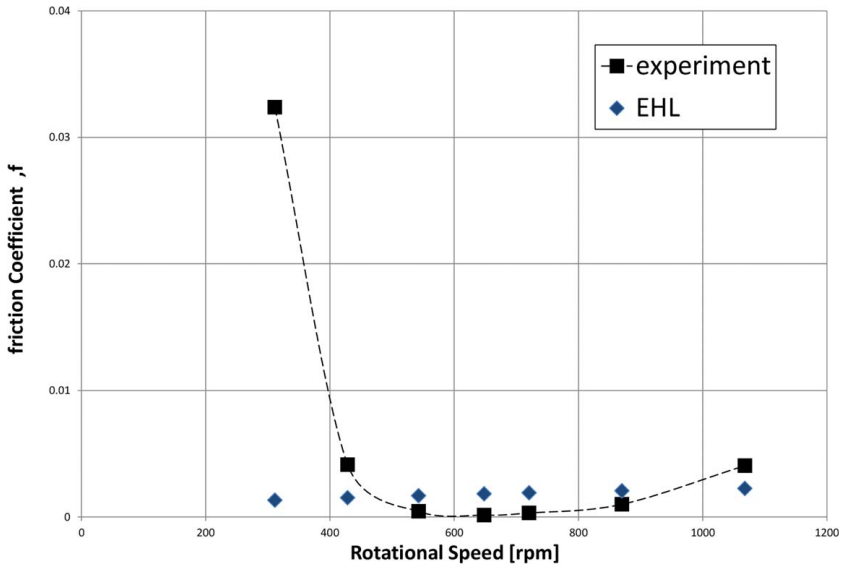


**Fig. 14 Coefficient of friction measurements versus EHL model prediction for nominal load for the experimental bearing**

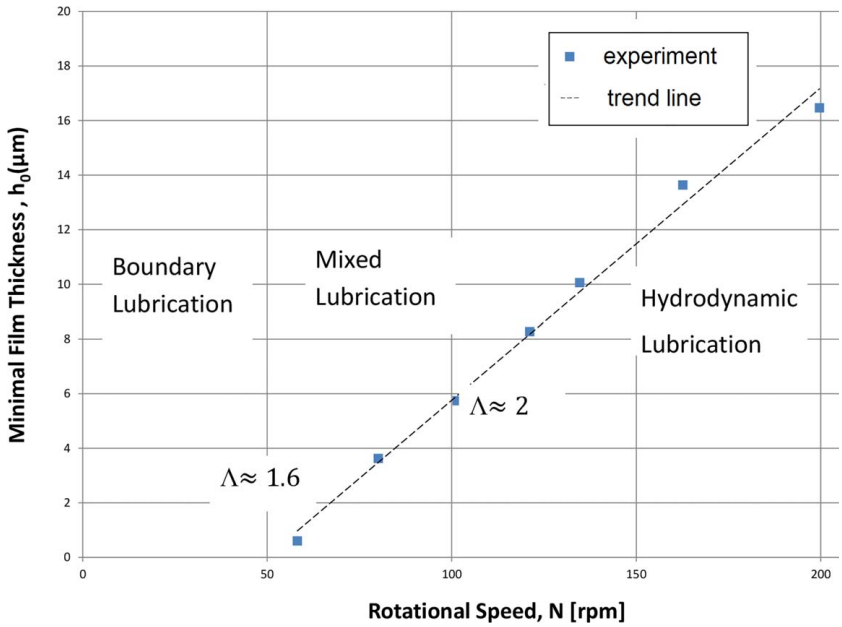


**Fig. 15 Minimal film thickness ($h_0$) versus rotational speed ($N$) for the vessel's bearing**

match between the calculated and experimentally obtained values for the friction coefficient was obtained. In the range of 500–1100 rpm, the maximum error between the friction coefficients was 0.001. It should also be noted that qualitatively, the behaviors of the experimental and computed friction coefficients are similar—a moderate, monotonic increase of the friction coefficient values as the shaft rotational speed increases to above 900 rpm.

Based on the experimentally obtained results for the scaled bearing and employing the similarity concept previously presented, the operation of the full-size vessel's bearing was evaluated. The film thickness versus shaft rotational speed as experimentally obtained and presented in Fig. 13 was transformed into the full-size bearing and is presented in Fig. 15. Based on the critical film thickness coefficient (inception of the full hydrodynamic regime at $\Lambda \geq 2$) as previously obtained, it is estimated that the vessel's bearing will operate in the full hydrodynamic regime only for rotational speeds above 100 rpm. This finding somehow contradicts the vessel's original design where it was estimated that the bearing would operate in the full hydrodynamic regime throughout the whole shaft rotational speed range.

This finding is backed by the emitted noise and the wear observed on the vessel's bearing when operated in the lower rotational speed range. To overcome this problem, an increase in the bearing load carrying capacity is necessary. As neither increasing the propeller shaft diameter nor increasing the bearing length is feasible, it seems that an increase in the angular sector of the bearing may offer a realistic solution. Employing the developed EHL model and the experimental finding for the full hydrodynamic regime inception ($\Lambda \geq 2$), it was calculated that increasing the angular sector by 80 deg–180 deg will allow the development of a full hydrodynamic film at a rotational speed of 60 rpm speed, which is relatively close to the lower operational speed of the shaft.

Surface texturing may be also a possible solution to increase the bearing's load carrying capacity.

## 5 Conclusions

Water-lubricated journal bearings are an important component in the propulsion systems of modern vessels, and their flawless operation is of a critical importance in vessel reliability. In the present study, a water-lubricated polymer bearing was investigated both analytically and experimentally. Based on torque and clearance measurements, zones for the bearing's operation in the different lubrication regimes were postulated. The experimentally obtained clearance was compared with the computed clearance, and a good match was observed with the bearing operating in the full hydrodynamic lubrication regime.

Contrary to the vessel's original design, we found that the bearing does not operate in the full hydrodynamic lubrication regime at all shaft operational speeds. This finding may explain the emitted noise when the vessel's shaft is operated at slow rotational speeds and the observed wear. It was also observed that for this type of water-lubricated journal bearing, the full hydrodynamic regime may already be reached at a minimum film thickness coefficient of $\Lambda \approx 2$ rather than as commonly mentioned in the literature for metal journal bearings, $\Lambda \geq 3$. Given that the preference is for the bearing to operate in the full hydrodynamic lubrication regime at all shaft rotational speeds, the bearing's load carrying capacity should be increased. Theoretically, this can be achieved by increasing the bearing length; unfortunately, this option is practically unfeasible as it requires extensive changes in the vessel's design. Consequently, in a future work, options for increasing the bearing's angular sector and for applying surface texturing to obtain an adequate increase in the load carrying capacity will be investigated.


## Acknowledgment

The authors are grateful to Dr. Yuri Kligerman from the Faculty of Mechanical Engineering, Technion–Israel Institute Technology, for his knowledgeable support.


## Conflict of Interest

There are no conflicts of interest.

## Nomenclature

$e$ = eccentricity (m)
$f$ = bearing friction coefficient
$h$ = nominal film thickness ($\mu$m)
$p$ = pressure (Pa)
$r$ = journal radius (m)
$u$ = displacement vector
S = Sommerfeld number (–)
$C$ = radial clearance (m)
$L$ = bearing's axial length (m)
$N$ = journal rotational speed (rpm)
$R$ = bearing's radius (m)
$U$ = surface velocity (m/s)
$W$ = load (kg)
$h_0$ = minimum film thickness ($\mu$m)
$h^*$ = modified local film thickness ($\mu$m)
$P_{av}$ = average pressure (Pa)
$P_{cav}$ = cavitation pressure (Pa)
$P_s$ = ambient pressure (Pa)
$R_b$ = surface roughness of bearing surface ($\mu$m)
$R_j$ = surface roughness of journal surface ($\mu$m)
$\varepsilon$ = dimensionless eccentricity (–)
$\theta$ = circumferential coordinate (rad)
$\theta_{cav}$ = cavitation angle (rad)
$\theta_{end}$ = partial bearing angular angle end (rad)
$\theta_{start}$ = partial bearing angular angle start (rad)
$\varnothing$ = attitude angle (rad)
$\lambda$ = length-to-diameter ratio (–)
$\Lambda$ = film thickness coefficient (–)
$\mu$ = lubricant viscosity (Pa s)
$\nu$ = Poisson's ratio (–)
$\rho$ = lubricant density (kg/m$^3$)

## References


[1] Pai, R., and Hargreaves, D. J., 2012, *Green Energy and Technology*, Springer, Heidelberg, Berlin, Chap. 13.
[2] Hirani, H., and Verma, M., 2009, "Tribological Study of Elastomeric Bearings for Marine Propeller Shaft System," Tribol. Int., **42**(2), pp. 378–390.
[3] Hongling, Q., Chang, Y., Hefa, Z., Xufei, L., Zhixiong, L., and Xiang, X., 2020, "Experimental Analysis on Friction-Induced Vibration of Water-Lubricated Bearings in a Submarine Propulsion System," Ocean Eng., **203**, p. 107239.
[4] Xie, Z., and Liu, H., 2020, "Experimental Research on the Interface Lubrication Regimes Transition of Water Lubricated Bearing," Mech. Syst. Sig. Process., **136**, p. 106522.
[5] Khonsari, M. M., and Booser, E. R., 2017, *Applied Tribology: Bearing Design and Lubrication*, 3rd ed., John Wiley & Sons, Hoboken, NJ.
[6] Bonneau, D., Fatu, A., and Souchet, D., 2014, *Mixed Lubrication in Hydrodynamic Bearings*, ISTE Ltd, London, UK and John Wiley & Sons, Hoboken, NJ.
[7] Litwin, W., 2009, "Water-Lubricated Bearings of Ship Propeller Shafts-Problems, Experimental Tests and Theoretical Investigations," Pol. Marit. Res., **16**(4), pp. 41–49.
[8] Oh, K. P., and Huebner, K. H., 1973, "Solution of the Elastohydrodynamic Finite Journal Bearing Problem," ASME J. Lubr. Technol., **95**(3), pp. 342–351.
[9] De Kraker, A., Van Ostayen, R. A., and Rixen, D. J., 2007, "Calculation of Stribeck Curves for (Water) Lubricated Journal Bearings," Tribol. Int., **40**(3), pp. 459–469.
[10] Xie, Z., Song, P., Hao, L., Shen, N., Zhu, W., Liu, H., and Tian, W., 2020, "Investigation on Effects of Fluid-Structure-Interaction (FSI) on the Lubrication Performances of Water Lubricated Bearing in Primary Circuit Loop System of Nuclear Power Plant," Ann. Nucl. Energy, **141**, p. 107355.
[11] Pinkus, O., and Sternlicht, B., 1961, *Theory of Hydrodynamic Lubrication*, McGraw-Hill Book Co, New York.
[12] Yu, T. S., and Szevi, A. Z., 1975, "Partial Journal Bearing Performance in the Laminar Regime," ASME. J. Lubr. Technol., **97**(1), pp. 94–100.
[13] Malik, M., Dass, B., and Sinhasan, R., 1983, "Performance Characteristics of a Centrally Loaded 120 Partial Journal Bearing Using Pseudoplastic Lubricants," Tribol. Int., **16**(1), pp. 9–16.
[14] Tower, B., 1985, "Second Report on Friction Experiments," Proc. Inst. Mech. Engrs., **36**(1), pp. 38–70.
[15] McKee, S. A., and McKee, T. R., 1932, "Pressure Distribution in Oil Films of Journal Bearings," Trans. ASME, **54**, pp. 149–165.
[16] McKee, S. A., White, H. S., and Swindells, J. F., 1948, "Measurements of Combined Frictional and Thermal Behavior in Journal-Bearing Lubrication," Trans. ASME, **70**, pp. 409–418.
[17] McKee, S. A., and White, H. S., 1950, "Oil Holes and Grooves in Plain Journal Bearings," Trans. ASME, **72**, pp. 1025–1034.
[18] Sprengel, J. F., and Hargreaves, D. J., 1990, "A Test Rig for the Performance Assessment of Non-Metallic Water Lubricated Bearings," International Tribology Conference, Barton, ACT, Australia, Dec. 3–5, pp. 91–96.
[19] Wang, N., Meng, Q., Wang, P., Geng, T., and Yuan, X., 2013, "Experimental Research on Film Pressure Distribution of Water-Lubricated Rubber Bearing With Multiaxial Grooves," ASME J. Fluids Eng., **135**(8), p. 084501.
[20] Litwin, W., 2010, "Influence of Main Design Parameters of Ship Propeller Shaft Water-Lubricated Bearings on Their Properties," Pol. Marit. Res., **17**(4), pp. 39–45.
[21] McCarthy, D. M. C., Glavatskih, S. B., and Byheden, Å, 2009, "Influence of Oil Type on the Performance Characteristics of a Two-Axial Groove Journal Bearing," Lubr. Sci., **21**(9), pp. 366–377.
[22] Litwin, W., 2019, "Marine Propeller Shaft Bearings Under Low-Speed Conditions: Water vs. Oil Lubrication," Tribol. Trans., **62**(5), pp. 839–849.
[23] Litwin, W., 2006, "The Test Stands for Water Lubricated Marine Main Shaft Bearings," The 12th Nordic Symposium on Tribology, DTU, Technical University of Denmark, Helsingor, Denmark.